

Three-dimensional lead iodide bromide perovskitoid with distinct photoelectric anisotropy

Zixian Yu, Kuan Kuang, Jie Yang, Junyuan Duan*, Mingkai Li,* Yunbin He,* Junnian Chen*

Ministry-of-Education Key Laboratory of Green Preparation and Application for Functional Materials, and School of Materials Science & Engineering, Hubei University, Wuhan 430062, China

*Corresponding authors.

E-mail addresses: chenjunnian910@hubu.edu.cn; ybhe@hubu.edu.cn.

KEYWORDS:

Experimental section

Materials. N-methyl-1,3-propanediamine (98%), hydrobromic acid solution (HBr, 48 wt.% in water), hydriodic acid solution (HI, AR, 45% wt.% in water), H_3PO_2 (AR, 50 wt.% in water) and $Pb(Ac)_2 \cdot 3H_2O$ (99.998%) were purchased from Aladdin Industrial Inc. All reagents were purchased from commercial vendors and used as received.

Synthesis of (NMPDA) Pb_2I_6 Single Crystals. Initially, 1 mmol of $Pb(Ac)_2 \cdot 3H_2O$ (0.3793 g) was dissolved in 5.5 mL of HI (45% wt.% in water) and 1 mL of H_3PO_2 solution while stirring at RT. Subsequently, 0.5mmol of N-methyl-1,3-propanediamine (53 μ L) was added directly to the previous mixture under stirring for a transparent yellow solution at 90°C in a methyl silicone oil bath. The precursor solution was then slowly cooled to RT for the growth of red crystals. Large single crystals were successfully grown from the saturated solution by the slow cooling process at a rate of 5 °C /day. The obtained single crystals were isolated and stored in a vacuum drying box.

Synthesis of (NMPDA) $Pb_2I_4Br_2$ Single Crystals. Initially, 2 mmol of $Pb(Ac)_2 \cdot 3H_2O$ (0.7586 g) was dissolved in 1.8mL of HI (45% wt.% in water) , 0.2 mL of H_3PO_2 and 7.2 mL HBr (48 wt.% in water) solution while stirring at RT. Subsequently, 1mmol of N-methyl-1,3-propanediamine (107 μ L) was added directly to the previous mixture under stirring for a transparent yellow solution at 90°C in a methyl silicone oil bath. Then the hot oversaturated solution was cooled down at a very slow rate of 5°C /day for the growth of orange crystals of (NMPDA) $Pb_2I_4Br_2$ The obtained single crystals were isolated and stored in a vacuum drying box.

Characterization. X-ray diffraction patterns (XRD) were recorded using a Bruker X-ray diffractometer (D8 ADVANCE) with $Cu K\alpha$ radiation ($\lambda = 1.54056 \text{ \AA}$). The absorption spectra were acquired with a UV–VIS–NIR spectrophotometer (UV-3600 Plus, SHIMADZU) using $BaSO_4$ powder as the reference. The absorption spectra were estimated from reflectance spectra by using the Kubelka–Munk function. The microscopic morphology of the crystals was acquired with a field emission SEM (Sigma500). The dielectric constants were measured at different frequencies using a TH 2832 LCR meter (Tonghui Electronic Co., Ltd in China). Scanning photocurrent

microscopy (SPCM) analysis was performed using a confocal Raman system (WITec, Alpha 300RS+), utilizing a continuous 532 nm laser at a laser intensity of 0.01 W/cm². Photocurrent is detected with a lock-in amplifier (FEMTO, DLPCA-200). Biases were collected by Keithley 2400 voltage source meter.

Fabrication and measurements of photodetectors. Photodetectors were fabricated by covering conductive silver paste on the surface of (NMPDA)Pb₂I₆ and (NMPDA)Pb₂I₄Br₂ single crystals. Current-voltage (*I*-V) and current-time (*I*-t) curves characteristics were recorded by a Keithley 2400 Source Meter. A 150 W low-pressure UV-enhanced xenon lamp was used as the light source and monochromatic light was obtained using a grating spectrometer. The optical power density was calibrated using a standard Si photodetector.

First-principles calculation methods. Based on the density functional theory (DFT), this research is carried out using the Vienna Ab Initio Simulation Package (VASP) codes. The Perdew-Burke-Ernzerhof (PBE) under generalized gradient approximation (GGA) functional is used to solve the interatomic exchange-correlation functional. The spin-orbit coupling (SOC) effect is adopted to optimize the band structure during the calculation, which introduces the effort of heavy element. For the computational parameters, the energy cutoff of projector augmented wave (PAW) set 500 eV. In addition, 6 × 3 × 8 and 3 × 6 × 8 k-point meshes are built for (NMPDA)Pb₂I₆ and (NMPDA)Pb₂I₄Br₂ in first Brillouin zone integration. The values of energy and force convergence were 10⁻⁶ eV and 0.01 eV/Å, respectively. Crystal explorer program is used to discuss the interaction between H atoms and other atoms around the organic cation.

We thereafter conducted SPCM characterization to map the photocurrent distribution in the lateral Ag/perovskitoid SC/Ag device for investigating the carrier diffusion behavior. The charge carriers of the perovskite device are locally excited by a mobile laser with 532 nm continuous wave and 0.3–0.4 μm spot size. Upon the laser scan the device along x and y directions in 0.5 μm increments, the instant photocurrent as a function of the laser position is recorded to form a photocurrent map.

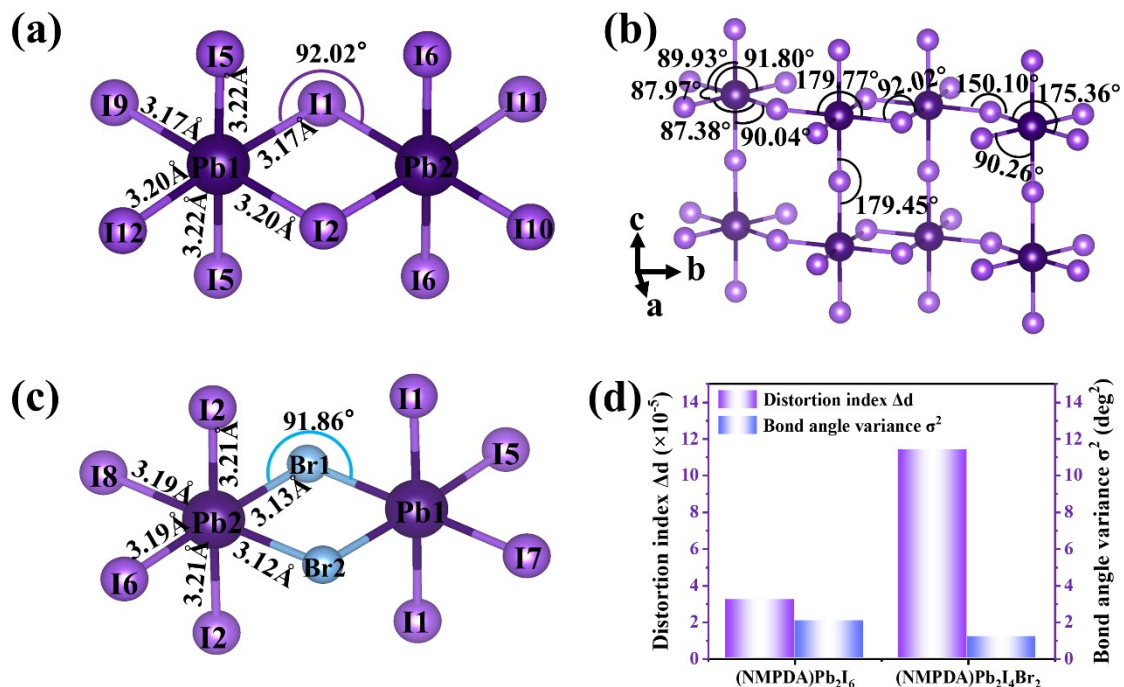


Figure S1. The crystal structure shows detailed bond length in (a) (NMPDA)Pb₂I₆ and (c) (NMPDA)Pb₂I₄Br₂. Packing view of the crystal structure along the a-axis of (NMPDA)Pb₂I₆. (d) The Pb-X bond length distortion (Δd) and Pb-X-Pb bond-angle variance (σ^2) of PbX₆ octahedron for (NMPDA)Pb₂I₆ and (NMPDA)Pb₂I₄Br₂.

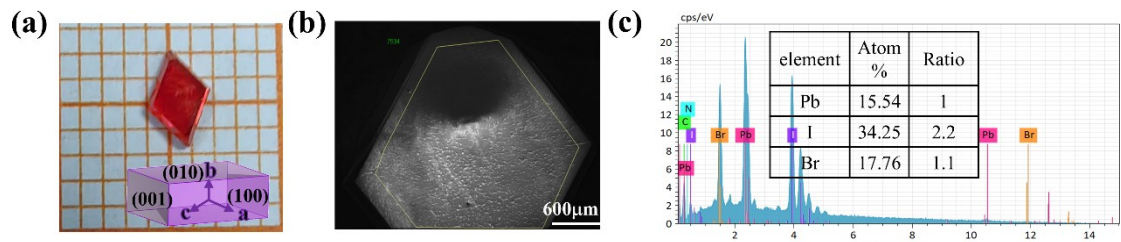


Figure S2. Photo and simulated morphology of (a) (NMPDA)Pb₂I₄Br₂ Crystal. (b) The selected area for EDS analysis in (NMPDA)Pb₂I₄Br₂. (c) EDS spectra of the detected elements Pb, I and Br. The C and N content is hard to accurately detect because of their small relative atomic masses.

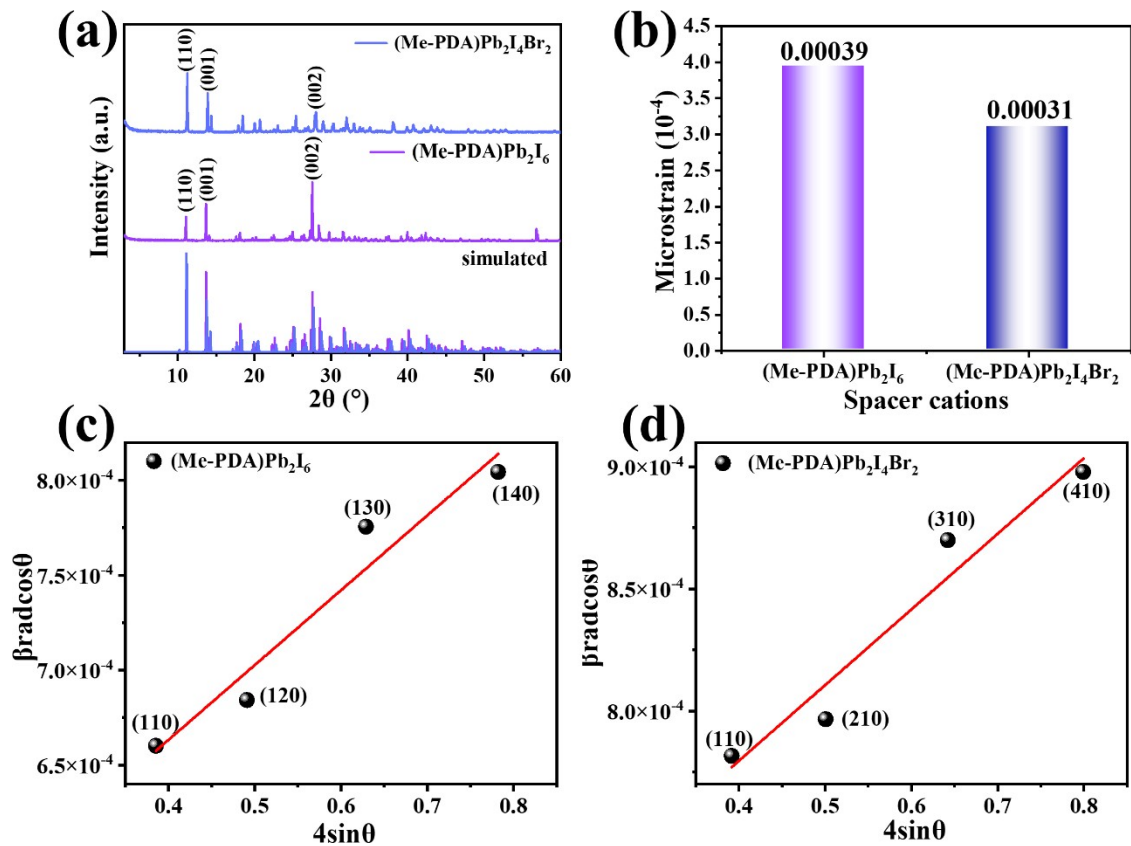


Figure S3. (a) XRD patterns of $(\text{NMPDA})\text{Pb}_2\text{I}_6$ and $(\text{NMPDA})\text{Pb}_2\text{I}_4\text{Br}_2$. (b) The microstrain of $(\text{NMPDA})\text{Pb}_2\text{I}_6$ and $(\text{NMPDA})\text{Pb}_2\text{I}_4\text{Br}_2$ derived from the W–H analysis. The Williamson–Hall (WH) plots of (c) $(\text{NMPDA})\text{Pb}_2\text{I}_6$ and (d) $(\text{NMPDA})\text{Pb}_2\text{I}_4\text{Br}_2$ deriving from XRD patterns according to $\beta \cos \theta = 4\epsilon \sin \theta + k\lambda/L$. The microstrain (ϵ) can be extracted from the line's slope.

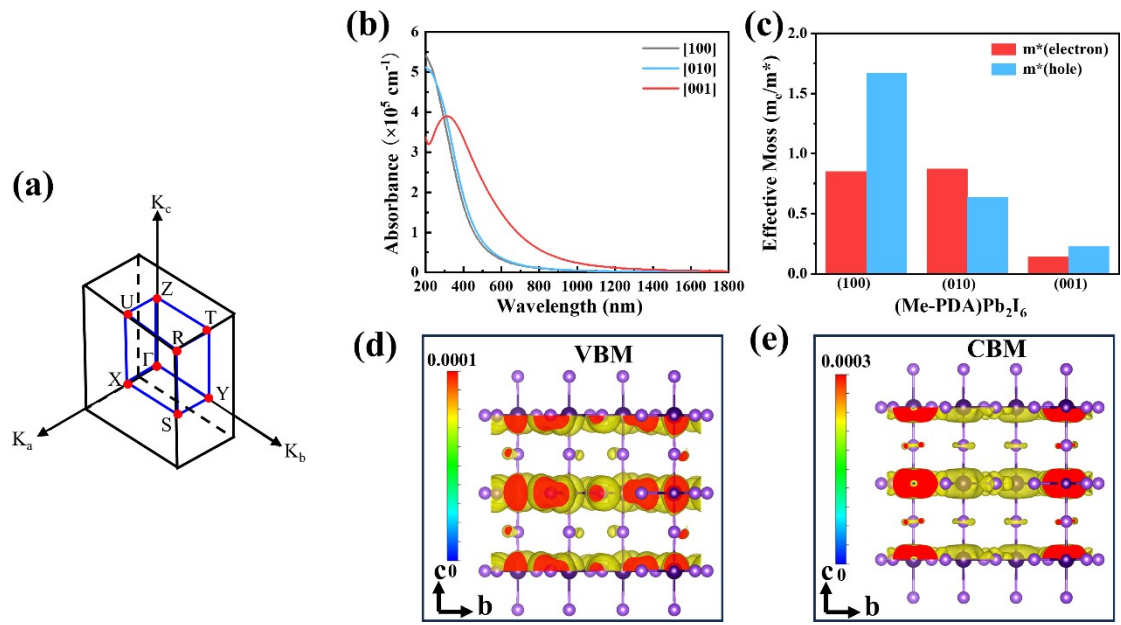


Figure S4. Figure S4. (a) Brillouin zone showing the k-path of (NMPDA)Pb₂I₆. (b) The calculated absorption coefficient for (NMPDA)Pb₂I₆. (c) The calculated carrier effective masses along different crystal axis of (NMPDA)Pb₂I₆. The isosurface plots of the (d) VBM and (e) CBM-associated charge density along the [001] direction of (NMPDA)Pb₂I₆.

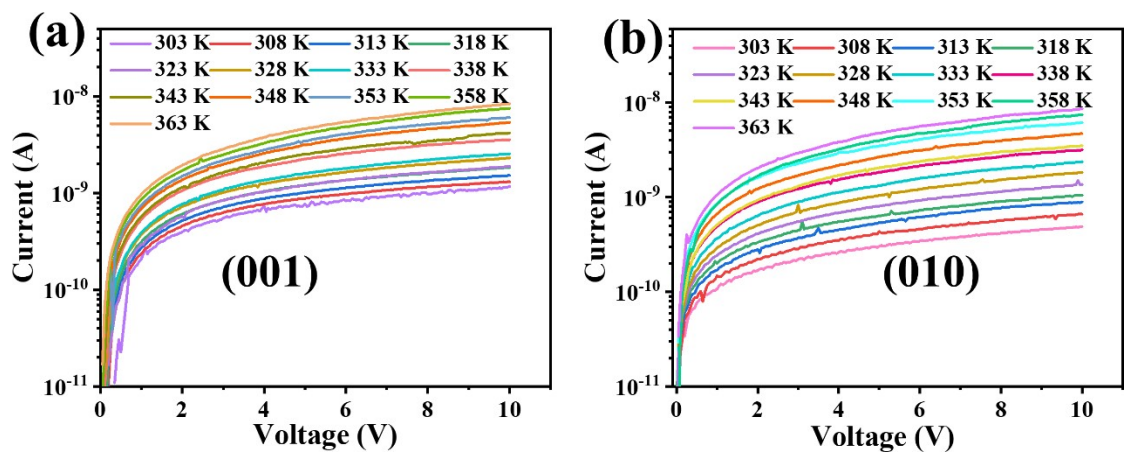


Figure S5. Temperature-dependent dark I - V curves along the (a) [010] and (b) [001] direction of $(\text{NMPDA})\text{Pb}_2\text{I}_4\text{Br}_2$.

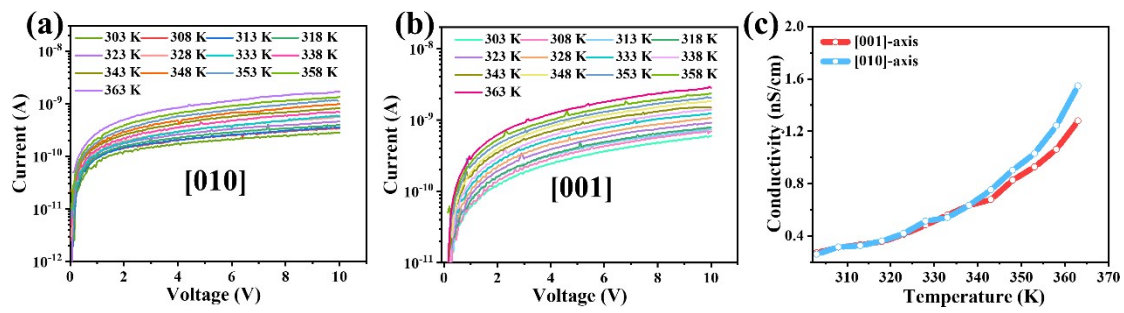


Figure S6. Temperature-dependent dark I - V curves along the (a) [010] and (b) [001] direction of (NMPDA)Pb₂I₆ single crystal. (c) Temperature-dependent electrical conductivity of (NMPDA)Pb₂I₆.

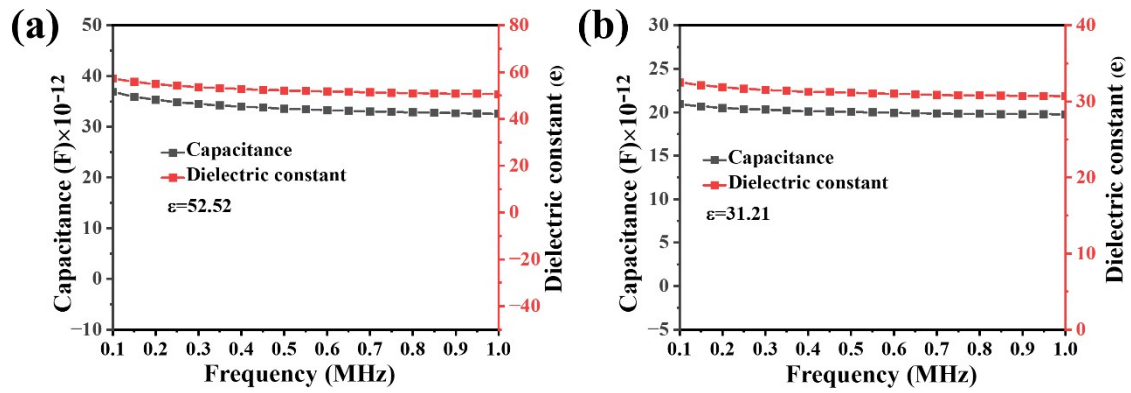


Figure S7. Frequency-dependent capacitance and dielectric constant curves of (a) (NMPDA)Pb₂I₆ and (b) (NMPDA)Pb₂I₄Br₂. The dielectric constants of (NMPDA)Pb₂I₆ and (NMPDA)Pb₂I₄Br₂ are calculated to be 52.52 and 31.21.

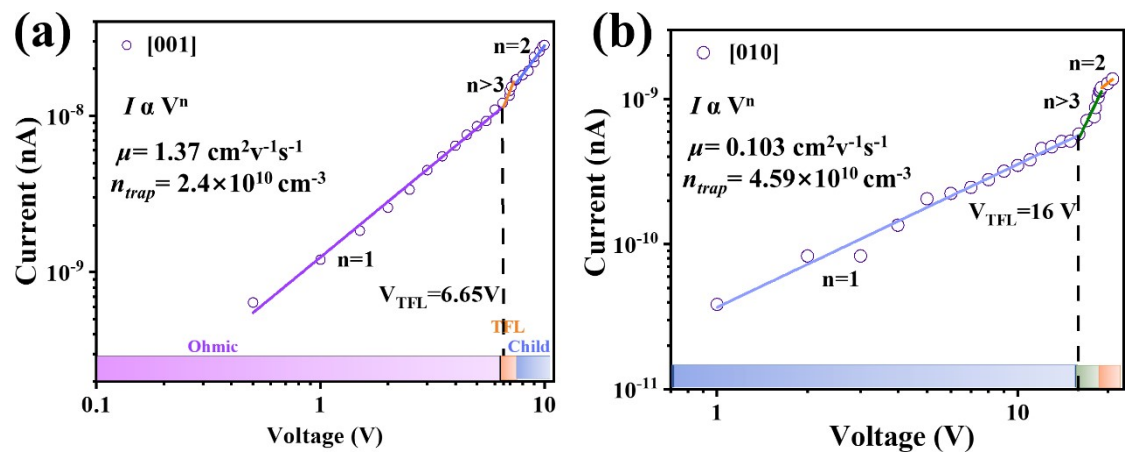


Figure S8. Logarithmic I - V curve along the (a) [001] and (b) [010] axis of (NMPDA) Pb_2I_6 .

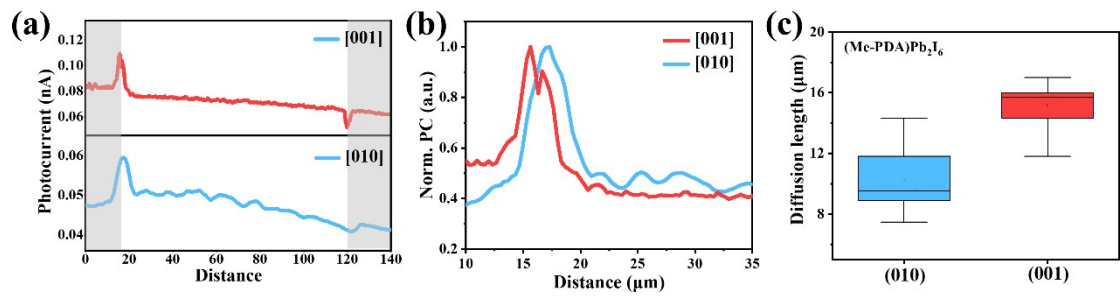


Figure S9. (a) Photocurrent line scans for (NMPDA)Pb₂I₆ single crystal device. (b) Normalized photocurrent line scans for (NMPDA)Pb₂I₆ device. (c) Boxplot of diffusion lengths extracted from the decaying photocurrent line scan.

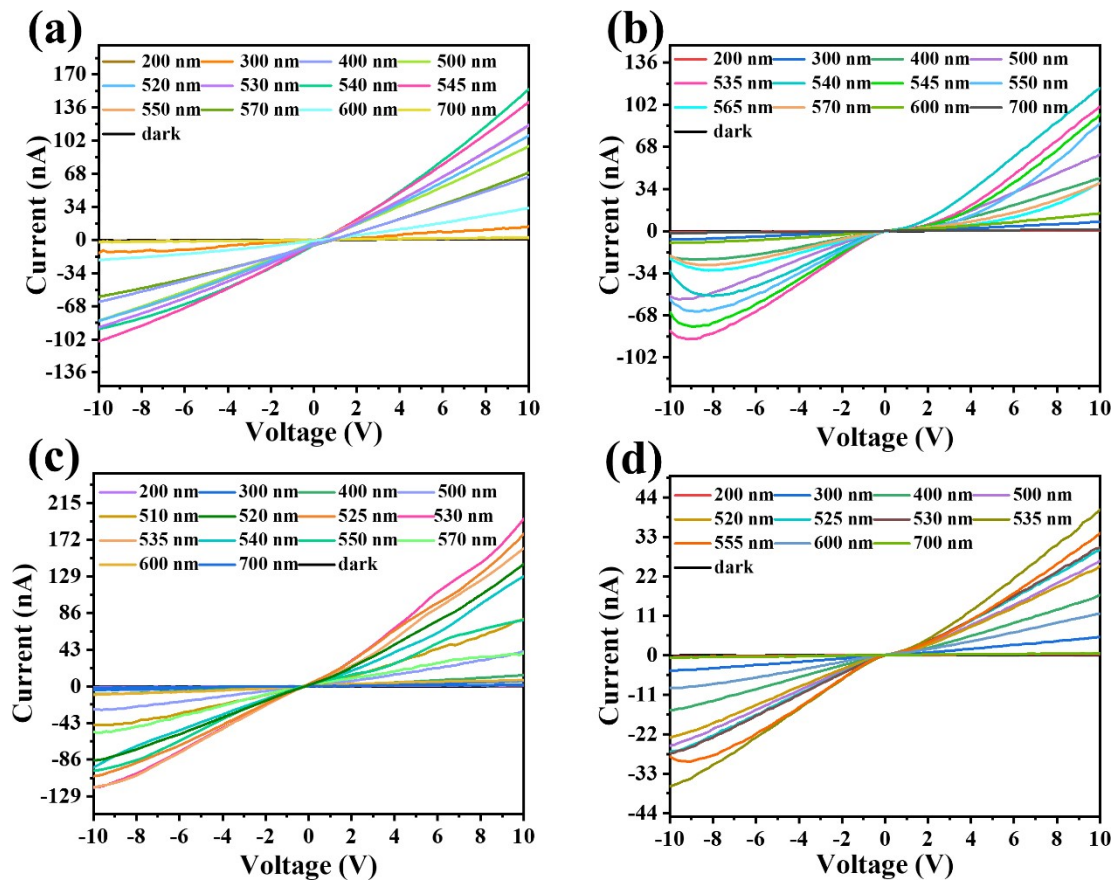


Figure S10. Wavelength-dependent I - V curve along the (a) [001] and (b) [010] axis of (NMPDA) Pb_2I_6 . Wavelength-dependent I - V curve along the (c) [001] and (b) [010] axis of (NMPDA) $\text{Pb}_2\text{I}_4\text{Br}_2$.

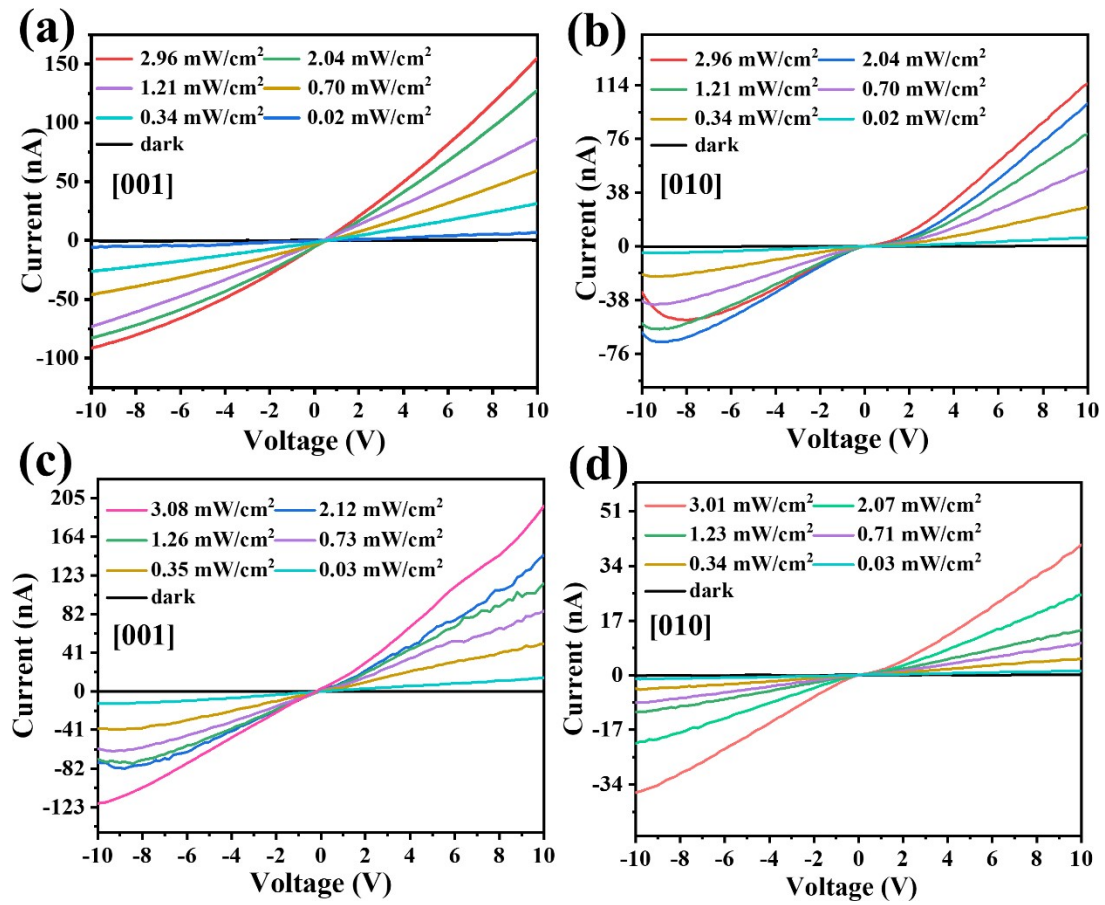


Figure S11. Optical power density-dependent I – V curve of $(\text{NMPDA})\text{Pb}_2\text{I}_6$ along the (a) [001] and (b) [010] direction under 540 nm irradiation. Optical power density-dependent I – V curve of $(\text{NMPDA})\text{Pb}_2\text{I}_4\text{Br}_2$ along the (c) [001] and (d) [010] axis under 530 and 525 nm irradiation.

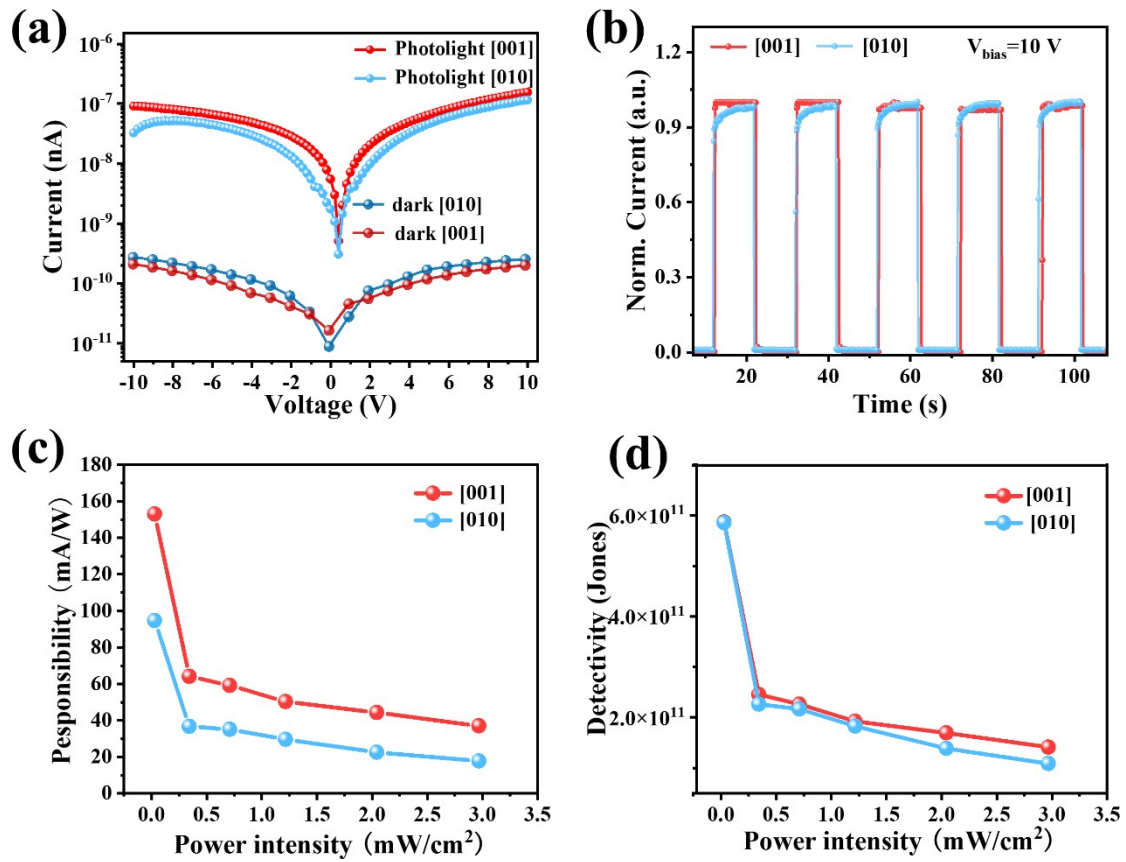


Figure S12. (a) $I-V$ curve of (NMPDA) Pb_2I_6 single crystal detector along different crystal axis measured in the dark and under light illumination. Temporal photoresponse of (b) (NMPDA) Pb_2I_6 single crystal detector along different crystal axis. (c) Responsivity and (d) detectivity of (NMPDA) Pb_2I_6 single crystal device along different crystal axis.

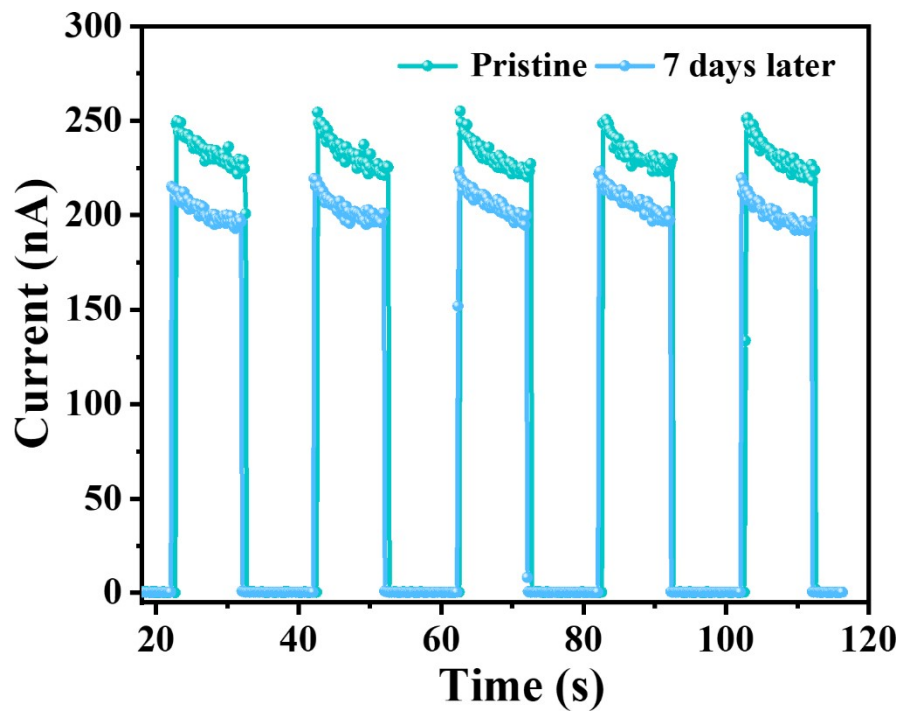


Figure S13. Time resolved photoresponse of the (NMPDA) $\text{Pb}_2\text{I}_4\text{Br}_2$ device after storage for a week under ambient atmosphere.

Table S1. Performance comparison of photodetectors based on the fabricated (NMPDA)Pb₂I₄Br₂ perovskite and other perovskites.

| Device | Bias (V) | Spectral responsivity (mA/W) | Detectivity (Jones) | Photocurrent (nA) | Darkcurrent (nA) | On/Off ratio | Rise time (ms) | Decay time (ms) | Reference |
|---|----------|------------------------------|-----------------------|-------------------|------------------|--------------|----------------|-----------------|-----------|
| (BMI)Pb ₂ I ₆ | 10 | 0.1 | 1.1×10^{10} | 1.3 | 0.28 | / | 1 | 0.8 | [28] |
| (DMEN)Pb ₂ I ₆ ·H ₂ O | 30 | 5.6 | 3.6×10^8 | 0.73 | / | / | / | / | [29] |
| (C ₆ H ₁₀ N ₂)Pb ₂ Br ₆ | 10 | 4 | 4×10^{10} | 14 | 0.0035 | $>10^3$ | 0.27 7 | 0.31 6 | [12] |
| (M ₂ pda)Pb ₂ I ₆ (c-axis) | 10 | 120 | / | / | / | >400 0 | / | / | [15] |
| (Mpda)Pb ₂ I ₆ | 10 | / | / | / | / | 1000 | / | / | [15] |
| (NMPDA)Pb ₂ I ₆ | 10 | 34.3 | 4×10^{11} | 26.3 | 0.02299 | 1144 | 28 | 46 | [17] |
| (NMPDA)Pb ₂ I ₄ Br ₂ | 10 | 280 | $3.05 \times 10_{12}$ | 116.59 | 0.04249 | 3920 | 30.2 | 36.7 | [17] |
| (NMDAP)Pb ₂ Br ₆ (c-axis) | 10 | 280 | $2.12 \times 10_{12}$ | 33 | 11 pA | 10^3 | 32 | 35 | [30] |
| (NMPDA)Pb ₂ I ₆ (c-axis) | 10 | 153 | $5.86 \times 10_{12}$ | 155 | 0.026 | 861 | 0.43 2 | 0.49 8 | This work |
| (NMPDA)Pb ₂ I ₄ Br ₂ (c-axis) | 10 | 401 | $4.85 \times 10_{12}$ | 198 | 0.018 | 7615 | 0.18 7 | 0.23 5 | This work |